Available online at www.sciencedirect.com

SciVerse ScienceDirect

Ceramics International 39 (2013) 5659–5665

CERAMICS INTERNATIONAL

www.elsevier.com/locate/ceramint

Synthesis of hematite and iron oxyhydroxide nanocrystals by precipitation of Fe^{3+} ions inside oleic acid micelles

N. Jović[a,*], N. Cvjetićanin[b], B. Babić-Stojić[a], D. Makovec[c], V. Jokanović[a]

[a]*Vinča Institute of Nuclear Sciences, University of Belgrade, P.O. Box 522, 11001 Belgrade, Serbia*
[b]*Faculty of Physical Chemistry, University of Belgrade, Studentski trg 12-16, 11158 Belgrade 118, Serbia*
[c]*Jožef Stefan Institute, Jamova 39, SI-1000 Ljubljana, Slovenia*

Received 2 November 2012; received in revised form 13 December 2012; accepted 24 December 2012
Available online 2 January 2013

Abstract

α-Fe_2O_3 nanospheres with diameters of 20–40 nm and FeOOH nanorods with diameters of 150–200 nm and lengths of 0.5–1.0 μm were synthesized via hydrolysis of $Fe(NO_3)_3$ and $FeCl_3$ solutions, respectively, in the presence of urea and oleic acid, under reflux at temperature ~90 °C for 8 h. The molar ratio of Fe^{3+} ions and urea were changed until pure phases have been obtained. The key parameter of the synthesis which provides pure hematite and β-FeOOH phases was the pH. The samples were characterized by X-ray powder diffraction, transmission electron microscopy and Mössbauer spectroscopy.

Keywords: B. Electron microscopy; C. Magnetic properties; D. Transition metal oxides

1. Introduction

Nanocrystalline and amorphous iron-rich systems such as iron oxides (Fe_2O_3, γ-Fe_2O_3, or Fe_3O_4) and iron oxyhydroxides (FeOOH) have many industrial and biomedical applications. Iron oxide nanoparticles are suitable for manufacturing of new electronic and optical devices, magnetic recording media, high density information storage devices, ferrofluids, catalysts, gas sensors, etc. [1,2]. Hematite as the most stable iron oxide phase can be used as a photoanode for water splitting [3], while its nano form possesses good catalytic properties [4]. Nanocrystalline hematite is an antiferromagnetic compound with very low saturation magnetization ($M_S \approx 1-2.5$ emu/g) and high Néel temperature ($T_N \sim 950$ K). On the contrary, Fe_3O_4 and γ-Fe_2O_3 nanoparticles (NPs) exhibit high magnetic saturation and good biocompatibility which make these systems attractive for biomedical applications (magnetic hyperthermia, magnetic resonance imaging, drug delivery) [5,6], and also, for the production of magnetic recording media [2]. Iron oxyhydroxides (FeOOH) can be used as adsorbents of toxic ions (Zn(II), Sb(III, V), As(III, V), U(IV), etc.) from water and soil, catalysts, electrode materials, or as precursors for different iron oxides [7–9].

Particle size, morphology, defect density, surface chemistry, inter- and intra-particle interactions have prevailing influence on electrical, magnetic and optical properties of nanomaterials. Therefore, it is important to establish carefully the synthesis conditions, which will yield the final product with desired properties.

By methods involving hydrolysis of ferrous (Fe^{2+}), and ferric (Fe^{3+}) ions in solutions, iron oxides, hydroxides, or iron oxyhydroxides can be obtained as final products, depending on the reaction conditions: temperature, pH value, presence of other ions in the solution (cations: Zn^{2+}, Ni^{2+}, Mn^{2+}, Al^{3+}, or anions: Cl^-, SO_4^{2-}, CO_3^{2-}), etc. [1,10]. Metastable ferrihydrite (a poorly crystalline oxide) represented by an approximate formula $FeOOH \cdot xH_2O$ usually appears as an intermediate phase in hydrolysis. Dehydratation of ferrihydrite under mildly acidic (pH ~ 3), or neutral conditions was found to favor the formation of hematite (α-Fe_2O_3) [10–12]. Upon heating, other iron oxides also yield the hematite phase as a final product [9,13].

Iron oxyhydroxides precipitate upon hydrolysis from different iron salt solutions. There are three different

*Corresponding author. Tel.: +381 11 8065 828; fax: +381 11 8065 829.
E-mail address: natasaj@vinca.rs (N. Jović).

0272-8842/$ - see front matter © 2013 Elsevier Ltd and Techna Group S.r.l. All rights reserved.
http://dx.doi.org/10.1016/j.ceramint.2012.12.082

polymorphic forms of FeOOH: goethite (α-FeOOH), akaganeite (β-FeOOH), and lepidocrocite (γ-FeOOH). Goethite is a common final product of the $Fe(NO_3)_3$ and $Fe_2(SO_4)_3$ salt hydrolysis, whereas akaganeite precipitates from $FeCl_3$ solution under strongly acidic conditions [14]. Chloride ions play a dominant role in tunnel akaganeite structure stabilization as described by *J.E. Post* and *V.F. Buchwald* [15]. The loss of chloride ions causes structural transformation to hematite phase [9]. Porous akaganeite structure, able to host water molecules, OH^-, or some other anions, transforms into: (i) dense α-Fe_2O_3 nanostructures unable to accommodate any ions [9], or (ii) very porous, hollow α-Fe_2O_3 nanostructures, able to store hydrogen and Li ions, or adsorb gases and heavy metal ions [16].

In this paper we investigated the product of precipitation of Fe^{3+} ions inside oleic acid micelles in the presence of urea when nitrate and chloride salts were used. The synthesis was performed by varying concentration of urea. Urea was used as a source of OH^- ions, enabling changes in the pH value in reaction, which has been shown as the key parameter in determining the purity of the final product. In certain papers, urea is considered as the chelating agent able to control size and morphology of the final product [17]. In addition, the synthesis of the materials inside oleic acid micelles was done because we expected that such obtained the hematite and akaganeite nanoparticles could have diverse morphologies, in agreement with investigations given in [18]. The morphology of the obtained nanoparticles was observed by TEM; their phase analysis and crystal structure were investigated by XRD, while magnetic behavior at room temperature was examined by Mössbauer spectroscopy.

2. Material and methods

2.1. Preparation

Nanocrystalline hematite and iron oxyhydroxide particles were synthesized by precipitation of Fe^{3+} ions inside oleic acid micelles, in the presence of urea ($(NH_2)_2CO$). The source of Fe^{3+} ions were $Fe(NO_3)_3 \cdot 9H_20$ and $FeCl_3 \cdot 6H_2O$ salts. All chemicals used in this synthesis were of analytical grade. Micelles were formed by ultrasonication of 0.5 ml of oleic acid and 100 ml of distilled water. Then, iron salt and urea were added into the solution. Their concentrations, as well as the samples label are given in Table 1. After stirring, the solution was transferred to a flask and maintained at 90–95 °C under reflux for 8 h. After cooling to room temperature, the pH of the suspension was monitored using pH meter. Then, a mixture of alcohol and acetone was added into the solution and centrifugated at a speed of 4000 rpm in order to separate the precipitates. In the next step, the obtained nanocrystals were washed with a mixture of hexane and ethyl alcohol several times (ratio: 78 mass% of hexane and 22 mass% of ethyl alcohol, in agreement with Hansen theory of solubility, briefly explained in Appendix A1) to eliminate the presence of oleic acid, and then dried at 60 °C.

Table 1
Experimental conditions in the synthesis of nanoparticles upon hydrolysis of Fe^{3+} ions in the presence of urea and oleic acid.

Sample	$Fe(NO_3)_3$ (mol/dm^3)	$FeCl_3$ (mol/dm^3)	$(NH_2)_2CO$ (mol/dm^3)	pH (final)	Phase identification
H_1	0.25		0.1	1.1	α-Fe_2O_3 + FeOOH
H_2	0.25		5.0	8.2	α-Fe_2O_3
A_1		0.25	0.1	1.3	α- + β- + γ-FeOOH
A_2		0.25	2.5	2.3	β-FeOOH

2.2. Characterization

X-ray powder diffraction (XRD) patterns were recorded using a Philips 1710 diffractometer, with CuKα radiation ($\lambda_{1,2}$ = 1.5406 Å), in the 2θ range of 8–76°, steps of 0.02°, and counting time of 15 s per step. The experimental XRD patterns were analyzed by FULLPROF program in a full profile-matching mode [19]. An average crystallite size of such obtained nanopowders was estimated from a line broadening using Scherrer's equation.

The morphology of the particles were observed by a transmission electron microscope (TEM, JEOL 2010 F) coupled with an EDXS microanalysis system (LINK ISIS EDS 300), operated at 200 kV. The samples were crashed, lightly milled in a mortar, suspended in acetone and deposited on a copper-grid-supported perforated transparent carbon foil.

Room temperature Mössbauer spectra of both samples were collected using an MS4 spectrometer with transmission geometry, operating in constant acceleration mode. Velocity calibration was done relative to natural iron foil. A ^{57}Co source in Rh matrix was used. The experimental data were fitted to Lorentzian lineshape using a least-square based method.

3. Results and discussion

3.1. Morphology and crystal structure analysis

The TEM images (a,b), and the electron diffraction patterns (c), of nanoparticles obtained by precipitation of Fe^{3+} ions upon hydrolysis of $Fe(NO_3)_3 \cdot 9H_20$ and $FeCl_3 \cdot 6H_2O$ salts, at $(NH_2)_2CO/Fe^{3+}$ molar ratio of 0.4, are shown in Figs. 1 and 2, respectively. It can be seen that the sample H_1, Fig. 1a, consists of open agglomerates of globular nanoparticles. Apart from globular nanoparticles, platelet or needle-like crystallites are also present. The globular nanoparticles are from 20 to 40 nm in size and composed of smaller crystallites, as evident from HRTEM image shown in Fig. 1b. The mean particle size, d_{TEM}, was found to be 24.1 nm (with the standard deviation 1.4 nm) (Fig. 1c). Electron diffraction pattern, Fig. 1c, taken at the

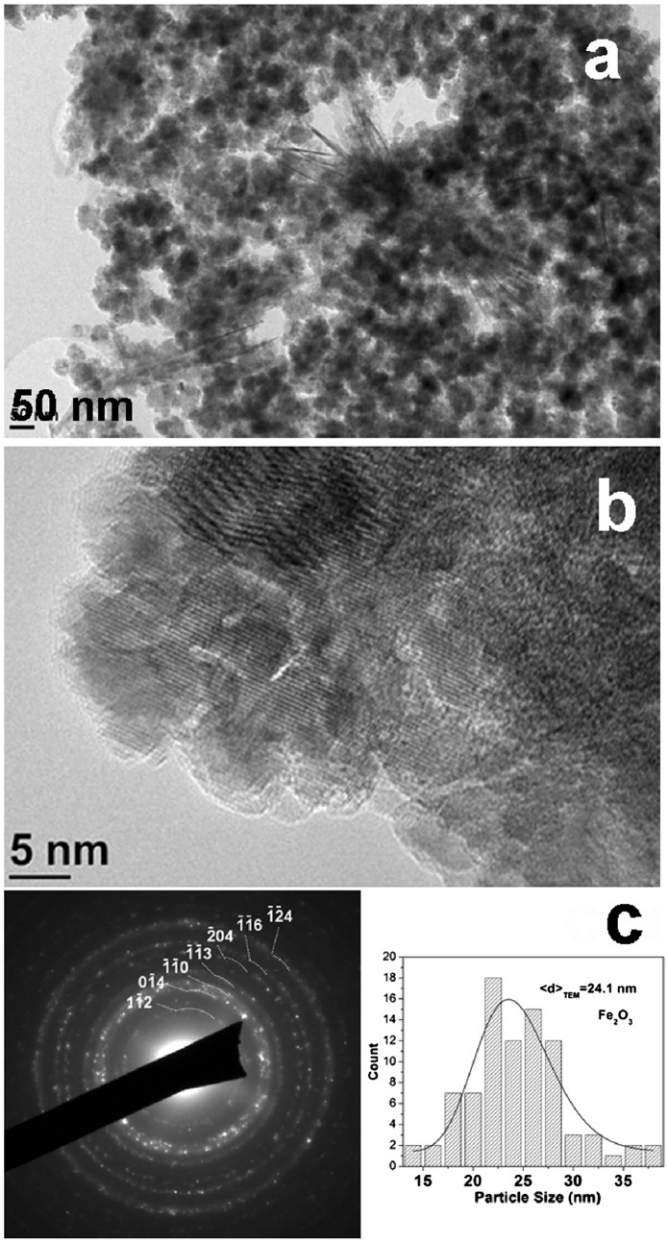

Fig. 1. (a,b) TEM imagines of sample H_1 (α-Fe_2O_3), and (c) the electron diffraction pattern and the particle size distribution.

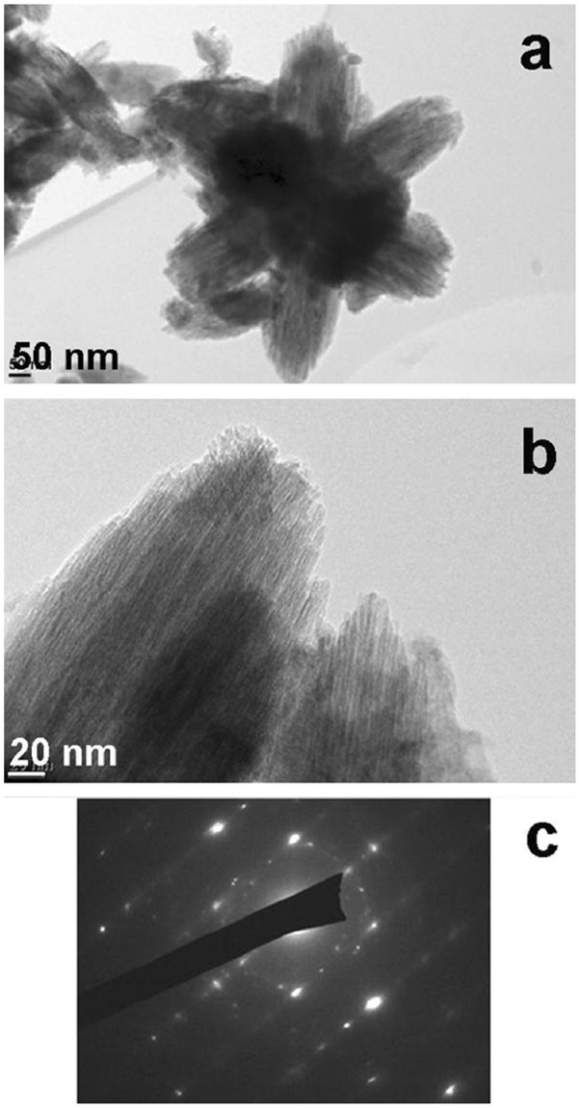

Fig. 2. (a,b) TEM imagines of sample A_1 (FeOOH), and (c) the electron diffraction pattern.

agglomerate of nanoparticles corresponds to hematite. The crystallites, which appear as needles (Fig. 1a) are visible at position where they are oriented with their large surfaces parallel to the electron beam. When they lie flat on the specimen support their contrast is quite weak, because they are very thin. They have a layered type structure, probably one of the FeOOH modifications.

TEM images of the sample A_1, Fig. 2, also reveal agglomerates, but of two types of nanoparticles: large, acicular nanoparticles, usually grouped in clusters looking like flowers, and small, more isotropic nanoparticles, Fig. 2a. The acicular nanoparticles are from approximately 500 nm to more than 1 μm long, and approximately 150–200 nm wide. They are poorly crystalline, Fig. 2c, and composed of much smaller, elongated nanoparticles, as can be seen in Fig. 2b. The layered type structure, observed in Fig. 2b probably corresponds to one of the FeOOH polymorphic forms.

XRD patterns of as prepared samples, H_1 and A_1, are shown in Fig. 3. The XRD pattern of sample H_1 corresponds to hematite (Fig. 3a), which is in accordance with the electron diffraction analysis. Almost all reflections were indexed in the space group (S.G.) $R\bar{3}c$ (Fig. 3a), in which the α-Fe_2O_3 phase crystallized. Additional reflection at $2\theta \sim 27^\circ$ can be a result of the presence of a small amount of iron oxyhydroxides (probably α-FeOOH). Broadened diffraction peaks indicate reduced crystallite size, as already observed by TEM. The average crystallite size value, d_{XRD}, was estimated using Scherrer's equation, $d_{XRD}=0.9\lambda/\beta\cos\theta$, where λ is the wavelength of X-rays, θ is the Bragg angle, and β is the full width at half maximum. Line broadening due to strain was neglected. From the line broadening of (104) and (116) reflections, the crystallite size was estimated to be about

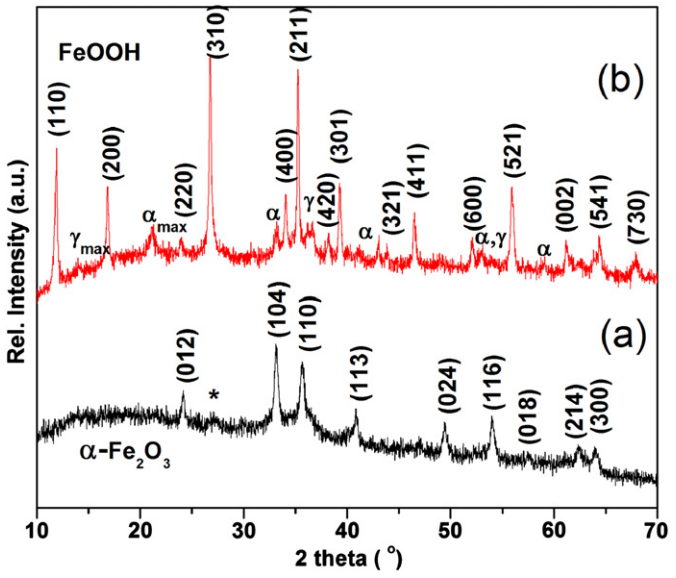

Fig. 3. XRD patterns of (a) sample H_1, and (b) sample A_1.

19 nm what is in accordance with the mean particle size value obtained from TEM.

The XRD analysis of the sample A_1 revealed a multi-phase final product, i.e. a mix of different FeOOH phases. The dominant phase was found to be akaganeite (β-FeOOH), while small amounts of goethite (α-FeOOH) and lepidocrocite (γ-FeOOH) are also present (Fig. 3b; the reflections with maximum intensity belonging to α-FeOOH and γ-FeOOH phases are denoted in the figure). Since the monoclinic distortion in β-FeOOH is usually very small, the crystal structure of akaganeite, instead in a monoclinic (S.G. *I*2/*m*), was considered in a tetragonal space group (S.G. *I*4/*m*) [15,20]. The unit cell parameters of all three phases: tetragonal β-FeOOH (S.G. *I*4/*m*), and orthorhombic α-FeOOH (S.G. *Pbnm*) and γ-FeOOH (S.G. *Cmcm*), were refined using the Rietveld method. The experimental and fitted XRD patterns for both samples are shown in Fig. 4, while the refined lattice parameters of all phases are summarized in Table 2. Good agreement between refined and literature data [15,16] were found.

As the XRD analysis shown, the products of hydrolysis of Fe^{3+} ions when the molar ratio of $(NH_2)_2CO/Fe^{3+}$ was kept at 0.4, were not pure, regardless nitrate or chloride iron salt was used. Therefore, in the next step, we tried to adjust the synthesis conditions by increasing the amount of urea in a following way: the molar ratio of $(NH_2)_2CO/Fe(NO_3)_3$ was set up to be 20, while the molar ratio of $(NH_2)_2CO/FeCl_3$ was 10 (see Table 1). The final pH values of the suspensions are also given in Table 1. The reaction temperature was kept unchanged (~90 °C). Eventual increasing in temperature could accelerate decomposing of urea, as well as the hydrolysis of Fe^{3+} ions in the presence of nitrate or chloride anions. The experimental and fitted XRD patterns of samples H_2 and A_2 are shown in Fig. 5. It can be seen that the new synthesis conditions enable getting pure α-Fe_2O_3 and β-FeOOH phases. Pure hematite phase is obtained from hydrolysis of

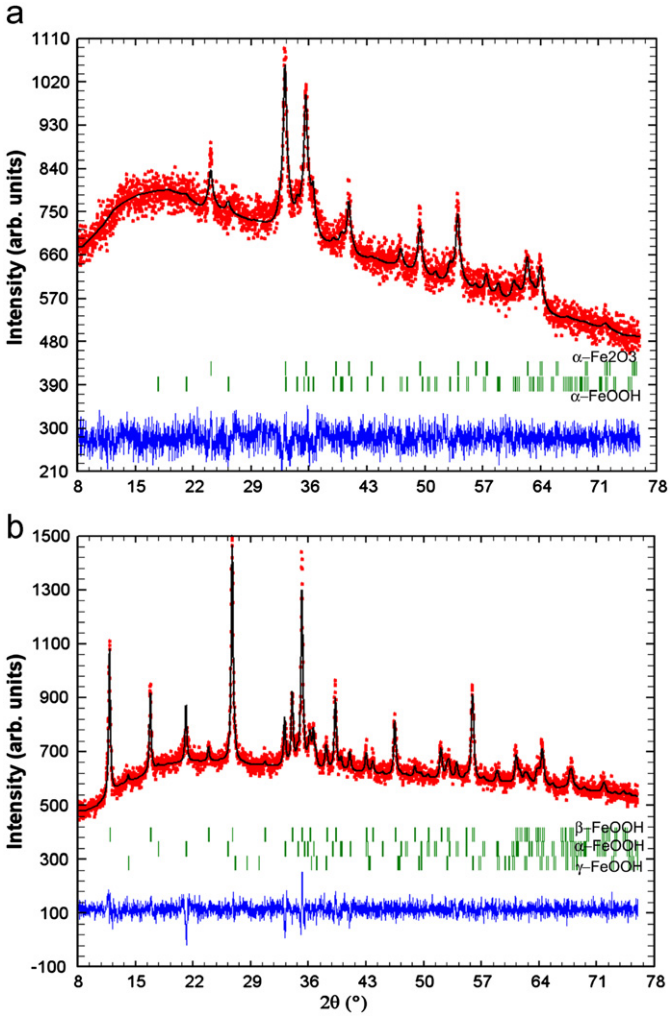

Fig. 4. Experimental (dots) and refined (line) XRD patterns of (a) sample H_1 and (b) sample A_1.

$Fe(NO_3)_3 \cdot 9H_2O$ salt at pH = 8.2 (mildly alkali environment), while pure akaganeite phase is formed upon hydrolysis of $FeCl_3 \cdot 6H_2O$ salt at pH = 2.3 (acidic environment). The refined lattice parameters of these samples are given in Table 2. From the line broadening of the strongest peaks, (104) and (110), the average size of α-Fe_2O_3 crystallites (sample H_2) was estimated to be about 29.5 nm, which is higher than value obtained for sample H_1 (d_{XRD} ~ 19 nm). We believe that, apart from the role to be source of OH^- ions (thus determining the pH), urea can influence the degree of crystallinity of nanoparticles and probably their size, by varying their concentration in the reaction. Such hypothesis is corroborated by recently published results [17,18].

3.2. Mössbauer spectra analysis

Room temperature Mössbauer spectra of samples H_1 and A_1 are shown in Fig. 6. Both samples exhibited superparamagnetic behavior at room temperature. The spectra were fitted with two doublets (components D1 and D2), while a broad singlet was introduced to delineate the baseline.

Table 2
Refined lattice parameters of the phases found in samples H_1, H_2, A_1 and A_2.

Sample	Phase	S.G.	Lattice parameters
H_1	α-Fe_2O_3	$R\bar{3}c$	$a=b=5.042(2)$ Å; $c=13.790(2)$ Å; $\alpha=\gamma=90°$; $\beta=120°$
	α-FeOOH	*Pbnm*	$a=4.628(1)$ Å; $b=9.997(11)$ Å; $c=3.036(3)$ Å; $\alpha=\beta=\gamma=90°$
H_2	α-Fe_2O_3	$R\bar{3}c$	$a=b=5.035(2)$ Å; $c=13.761(7)$ Å; $\alpha=\gamma=90°$; $\beta=120°$
A_1	β-FeOOH	*I4/m*	$a=b=10.565(1)$ Å; $c=3.029(1)$ Å; $\alpha=\beta=\gamma=90°$
	α-FeOOH	*Pbnm*	$a=4.626(1)$ Å; $b=9.996(1)$ Å; $c=3.022(1$ Å; $\alpha=\beta=\gamma=90°$
	γ-FeOOH	*Cmcm*	$a=3.068(1)$ Å; $b=12.527(1)$ Å; $c=3.865(1)$ Å; $\alpha=\beta=\gamma=90°$
A_2	β-FeOOH	*I4/m*	$a=b=10.571(2)$ Å; $c=3.033(1)$ Å; $\alpha=\beta=\gamma=90°$

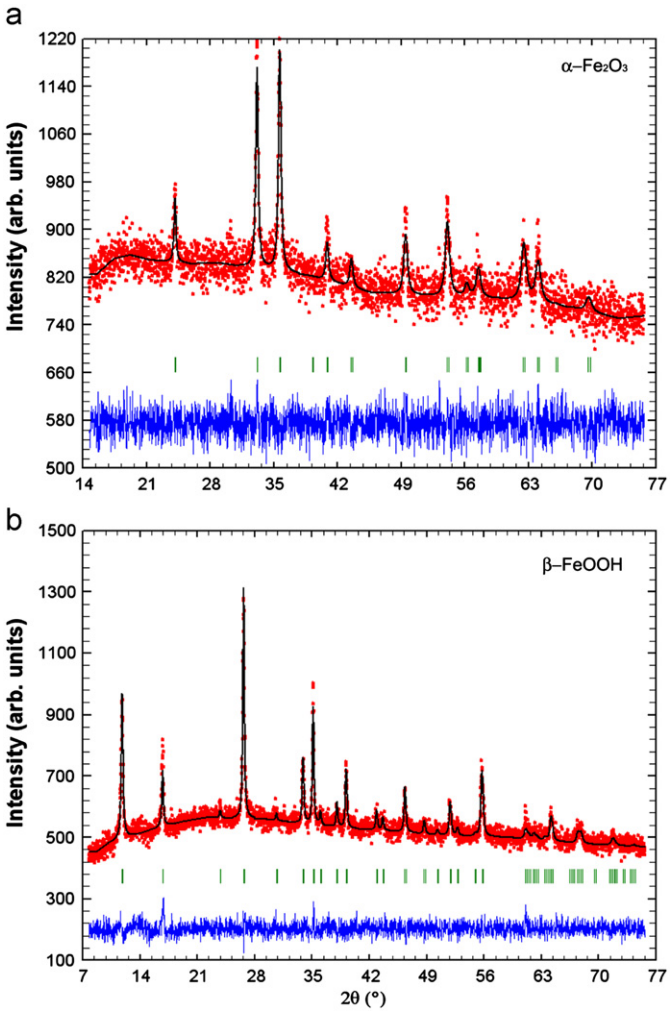

Fig. 5. Experimental (dots) and refined (line) XRD patterns of (a) sample H_2 and (b) sample A_2.

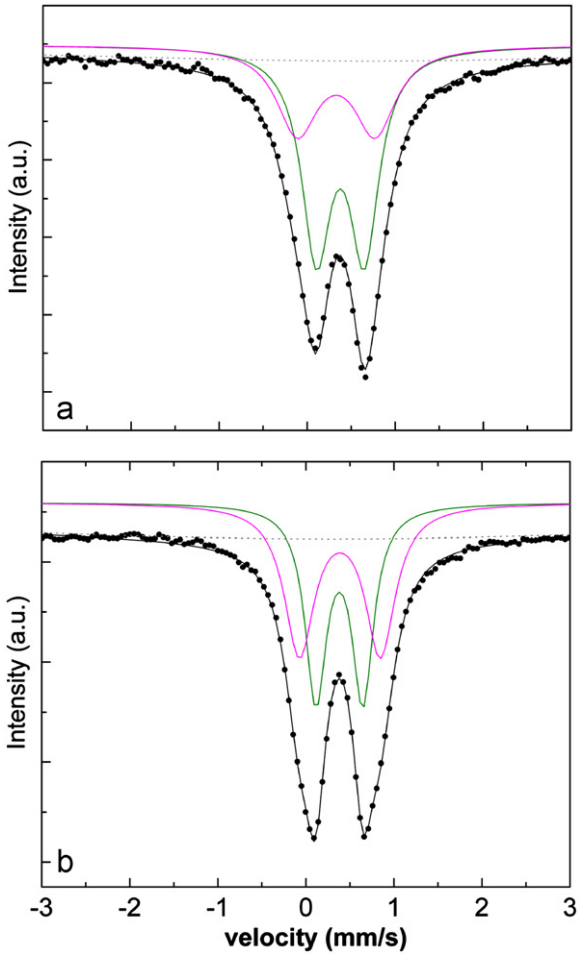

Fig. 6. Mössbauer spectra of: (a) sample H_1 (α-Fe_2O_3) and (b) sample A_1 (FeOOH), collected at room temperature.

The refined parameters of doublets D1 and D2 are given in Table 3. Superparamagnetic relaxations have already been observed in α-Fe_2O_3 NPs ~20-nm in size at room temperature [21]. It is well known that long-range dipole–dipole interactions are negligible in the assembly of α-Fe_2O_3 NPs due to their weak magnetic properties. Absence of magnetic hyperfine interactions [22] indicates that the possible exchange coupling between neighboring antiferromagnetic hematite NPs is suppressed due to particles coating [23]. Hematite nanoparticles are not in close contact with their neighbors probably because of the presence of oleic acid at particle surfaces. Oleic acid is an effective capping agent which stabilizes most ferrofluids. It has been found that the quadrupole splitting in the superparamagnetic state of hematite NPs takes value from interval $QS=0.51\pm0.03$ mm s^{-1}, and is practically independent of particles size [24]. Hence, the first component in Mössbauer spectra of sample H_1 can be unambiguously

Table 3
Mössbauer parameters: IS—isomer shift; QS—quadrupolar splliting, and Γ—linewidth, obtained by fitting the Mössbauer spectra of samples H_1 and A_1, collected at room temperature.

Sample	*Component*	*IS (mm/s)*	*QS (mm/s)*	*Γ (mm/s)*
H_1	D1	0.38	0.54 ± 0.01	0.20 ± 0.01
	D2	0.33	0.88 ± 0.01	0.28 ± 0.01
A_1	D1	0.38	0.53 ± 0.01	0.15 ± 0.01
	D2	0.38	0.92 ± 0.02	0.21 ± 0.01

assigned to the hematite phase. Since the product of synthesis via precipitation of Fe^{3+} ions in aqueous solution of $Fe(NO_3)_3$ precursor, in addition to α-Fe_2O_3 phase, contains some amount of FeOOH phase (as confirmed by XRD and TEM), the second component in Mössbauer spectra of sample H_1 could be attributed to these phases. It was found that the quadrupole splitting of the second phase is larger than the quadrupole splitting of superparamagnetic hematite.

The Mössbauer spectrum of sample A_1 was fitted with two symmetric doublets. The refined parameters, given in Table 3, are in agreement with the literature data for β-FeOOH [25]. The fractions of these two doublets (D1 and D2) have the same isomer shift value and a ratio close to 1:1, and, therefore, both components are assigned to Fe^{3+} ions centered in two distinct octahedra characteristic of β-FeOOH phase.

4. Conclusions

In this paper we investigated iron-rich nanoparticles obtained via hydrolysis of $Fe(NO_3)_3$ and $FeCl_3$ solutions, in the presence of urea, inside oleic acid micelles and under reflux at ~90 °C. The α-Fe_2O_3 and FeOOH nanoparticles were obtained during the precipitation, when nitrate and chloride salts were used, respectively. Pure hematite phase has been obtained at mildly alkali environment (pH = 8.3), while the formation of pure akaganeite phase is favorable in acidic conditions (pH = 2.3), in the high presence of chloride ions. It is postulated that the concentration of urea could influence the degree of crystallinity of nanoparticles. Different morphologies of NPs were observed, depending on the source of Fe^{3+} ions used. Hematite NPs are globular in shape and much smaller in size (20–40 nm) than FeOOH nanoparticles which are acicular, 150–200 nm in diameter and 0.5–1 μm long. Such morphologies are common for these materials. The possible influence on the morphology of nanoparticles due to the presence of oleic acid in solutions was not observed. Although, agglomerates of nanoparticles were observed in both samples, Mössbauer spectroscopy shows the absence of interparticle interactions at room temperature, probably due to adsorption of oleic acid at NP surfaces.

Acknowledgments

This work has been supported by the Ministry of Education, Science and Technological Development of the Republic of Serbia through the grant No. 172026. We thank Božana Čolović for help in synthesis.

Appendix A1. Oleic acid as a capping agent

For biological applications of magnetic NPs it is necessary they exhibit excellent stability in aqueous media, what requires their hydrophilic nature. Oleic acid (OA), when is bonded onto NPs surface, makes them hydrophobic. Many synthesis methods for production of monodispersed NPs with potential biomedical applications commonly use OA molecules. Therefore, the important step in getting biocompatible nanoparticles is making their surface hydrophilic. It can be done via ligand exchange (when OA molecules are replaces with some water miscible ones), or ligand adding process (when amphiphilic molecules, able to attached OA molecules, build addition surface layer). Recently has been shown that poly(ethylene glycol)-coated iron hydroxide nanoparticles (PEG/FeOOH) have potential application as magnetic resonance contrast agents [26]. It is known that oleic acid molecules are usually tightly bonded onto nanocrystals. For effective removement of OA, it is necessary to use solvent with appropriate coefficient of solubility. Following Hansen rule of selection [27] it is possible to select the most effective solvent or mixture of solvents, taking account that their resultant coefficient of solubility should be equal or almost equal to coefficient of solubility of corresponding polymer. For oleic acid the coefficient of solubility is 17.36 [28]. If hexane and ethyl alcohol are used as solvents, as in our case, the adequate mixture for washing OA should contain 0.78 mass% of hexane and 0.22 mass% of ethyl alcohol. For such mixture, the mutual coefficient of solubility 17.38 is almost equal to the coefficient of solubility of oleic acid [28].

References

[1] C. Wu, P. Yin, X. Zhu, C. Yang, Y. Xie, Synthesis of hematite (α-Fe_2o_3) nanorods: diameter-size and shape effects on their applications in magnetism, lithium ion battery, and gas sensors, Journal of Physical Chemistry B 110 (2006) 17806–17812.
[2] G.F. Goya, T.S. Berquo, F.C. Fonseca, M.P. Morales, Static and dynamic magnetic properties of spherical magnetite nanoparticles, Journal of Applied Physics 94 (2003) 3520–3528.
[3] J.H. Bang, K.S. Suslick, Sonochemical synthesis of nanosized hollow hematite, Journal of the American Chemical Society 129 (2007) 2242–2243.
[4] A. Brown, J. Hargreaves, B. Rijniersce, A study of the structural and catalytic effects of sulfation on iron oxide catalysts prepared from goethite and ferrihydrite precursors for methane oxidation, Catalysis Letters 53 (1998) 7–13.
[5] A. Figuerola, R. Di Corato, L. Manna, T. Pellegrino, From iron oxide nanoparticles towards advanced iron-based inorganic materials designed for biomedical applications, Pharmacological Research 62 (2010) 126–143.
[6] G.F. Goya, V. Grazú, M.R. Ibarra, Magnetic nanoparticles for cancer therapy, Current Nanoscience 4 (2008) 1–16.
[7] F. Kolbe, H. Weiss, P. Morgenstern, R. Wennrich, W. Lorenz, K. Schurk, H. Stanjek, B. Daus, Sorption of aqueous antimony and

arsenic species onto akaganeite, Journal of Colloid and Interface Sciences 357 (2011) 460–465.
[8] S. (Doyurum) Yusan, S. Akyil, Sorption of uranium(VI) from aqueous solutions by akaganeite, Journal of Hazardous Materials 160 (2008) 388–395.
[9] S. Musić, S. Krehula, S. Popović, Thermal decomposition of β-FeOOH, Materials Letters 58 (2004) 444–448.
[10] Y. Cudennec, A. Lecerf, The transformation of ferrihydrite into goethite or hematite, revisited, Journal of Solid State Chemistry 179 (2006) 716–722.
[11] B. Lu, P. Li, H. Liu, L. Zhao, Y. Wei, Synthesis of hexagonal pyramidal columnar hematite particles by a two-step solution route and their characterization, Powder Technology 215–216 (2012) 132–136.
[12] S. Lian, E. Wang, Z. Kang, Y. Bai, L. Gao, M. Jiang, C. Hu, L. Xu, Synthesis of magnetite nanorods and porous hematite nanorods, Solid State Communications 129 (2004) 485–490.
[13] R. Zboril, M. Mashlan, D. Petridis, Iron(III) oxides from thermal processess synthesis, structural and magnetic properties, Mössbauer spectroscopy characterization, and applications, Chemistry of Materials 14 (2002) 969–982.
[14] J. Cai, J. Liu, Z. Gao, A. Navrotsky, S.L. Suib, Synthesis and anion exchange of tunnel structure akaganeite, Chemistry of Materials 13 (2001) 4595–4602.
[15] J.E. Post, V.F. Buchwald, Crystal structure refinement of akaganéite, American Mineralogist 76 (1991) 272–277.
[16] J. Lian, X. Duan, J. Ma, P. Peng, T. Kim, W. Zheng, Hematite (α-Fe_2O_3) with various morphologies: ionic liquid-assisted synthesis, formation mechanism, and properties, ACS Nano 3 (2009) 3749–3761.
[17] M. Srivastava, J. Singh, M. Yashpal, A.K. Ojha, Synthesis, growth mechanism and characterization of single crystalline α-Fe_2O_3 spherical nanoparticles, Journal of Nanoscience and Nanotechnology 12 (2012) 6248–6257.
[18] X. Cao, L. Gu, Spindly cobalt ferrite nanocrystals: preparation, characterization and magnetic properties, Nanotechnology 16 (2005) 180–185.
[19] J. Rodriguez-Carvajal, FullProf computer program, 〈http://www.ill.eu/sites/fullprof/2009〉.
[20] J. Kim, C.P. Grey, ^{2}H and ^{7}Li solid-state MAS NMR study of local environments and lithium adsorption on the iron(III) oxyhydroxide, akaganeite (β-FeOOH), Chemistry of Materials 22 (2010) 5453–5462.
[21] M.F. Hansen, C.B. Koch, S. Mørup, Magnetic dynamics of weakly and strongly interacting hematite nanoparticles, Physical Review B 62 (2000) 1124–1135.
[22] N.M. Deraz, A. Alarifi, Novel processing and magnetic properties of hematite/maghemite nano-particles, Ceramics International 38 (2012) 4049–4055.
[23] C. Frandsen, S. Mørup, Spin Rotation in α-Fe_2O_3 nanoparticles by interparticle interactions, Physical Review Letters 94 (2005) 027202–027204.
[24] F. Bødker, S. Mørup, Size dependence of the properties of hematite nanoparticles, Europhysics Letters 52 (2000) 217.
[25] M. Zic, M. Ristic, S. Music, The effect of temperature on the crystallization of α-Fe_2O_3 particles from dense β-FeOOH suspensions, Materials Chemistry and Physics 120 (2010) 160–166.
[26] M. Kumagai, Y. Imai, T. Nakamura, Y. Yamasaki, M. Sekino, Sh. Ueno, K. Hanaoka, K. Kikuchi, T. Nagano, E. Kaneko, K. Shimokado, K. Kataoka, Iron hydroxide nanoparticles coated with poly(ethylene glycol)-poly(aspartic acid) block copolymer as novel magnetic resonance contrast agents for in vivo imaging, Colloid Surfaces B 56 (2007) 174–181.
[27] C.M. Hansen, The universality of the solubility parameter, Industrial and Engineering Chemistry Product Research and Development 8 (1969) 2–11.
[28] E. Stefanis, I. Tsivintzelis, C. Panayiotou, The partial solubility parameters: An equation-of-state approach, Fluid Phase Equilibria 240 (2006) 144–154.